Received: 6 April 2021 | Accepted: 13 May 2021

DOI: 10.1002/bit.27822

ARTICLE

BIOTECHNOLOGY AND BIOENGINEERING WILEY

A scalable bubble-free membrane aerator for biosurfactant production

Patrick Bongartz[1,2] | Isabel Bator[2,3] | Kristina Baitalow[1] | Robert Keller[1] | Till Tiso[3] | Lars Mathias Blank[3] | Matthias Wessling[1,4]

[1]Chemical Process Engineering (AVT.CVT), RWTH Aachen University, Aachen, Germany

[2]Bioeconomy Science Center (BioSC), Forschungszentrum Jülich, Jülich, Germany

[3]Institute of Applied Microbiology, Aachen Biology and Biotechnology, RWTH Aachen University, Aachen, Germany

[4]DWI Leibniz – Institute for Interactive Materials, Aachen, Germany

Correspondence

Dr. Matthias Wessling, DWI Leibniz – Institute for Interactive Materials, Forckenbeckstr. 50, 52074 Aachen, Germany.
Email: Manuscripts.CVT@avt.rwth-aachen.de

Funding information

RWTH Aachen University, Grant/Award Number: project thes0610; NRW Strategieprojekt BioSC, Grant/Award Number: No. 313/323-400-00213

Abstract

The bioeconomy is a paramount pillar in the mitigation of greenhouse gas emissions and climate change. Still, the industrialization of bioprocesses is limited by economical and technical obstacles. The synthesis of biosurfactants as advanced substitutes for crude-oil-based surfactants is often restrained by excessive foaming. We present the synergistic combination of simulations and experiments towards a reactor design of a submerged membrane module for the efficient bubble-free aeration of bioreactors. A digital twin of the combined bioreactor and membrane aeration module was created and the membrane arrangement was optimized in computational fluid dynamics studies with respect to fluid mixing. The optimized design was prototyped and tested in whole-cell biocatalysis to produce rhamnolipid biosurfactants from sugars. Without any foam formation, the new design enables a considerable higher space–time yield compared to previous studies with membrane modules. The design approach of this study is of generic nature beyond rhamnolipid production.

KEYWORDS

foam-free, membrane aeration, metabolic engineering, *Pseudomonas putida*, rhamnolipid

1 | INTRODUCTION

Traditional resources for the majority of surfactant precursors are crude oil or plant oil (Henkel et al., 2012). Even though, for example, palm oil is an organic source of surfactant precursors, the monocultural plantation of those plants is a bioecological threat (Cazzolla Gatti et al., 2019). Renewable carbon-rich waste streams of the agricultural industry can potentially replace these state-of-the-art precursors to create sustainable products via biotechnological routes (Henkel et al., 2012). Yet, conventional fermentation for the production of biosurfactants can encounter a major drawback, which reduces the overall process cost efficiency: Excessive foam formation (Kosaric & Sukan, 2014). Biosurfactants accumulate at the gas–liquid interphase and are discharged of the fermentation broth (Anic et al., 2018). The foam layer builds a barrier for gas exchange in the bioreactor's headspace. Additionally, the rapidly forming foam impedes process control (Fiechter, 1992). The amount of produced foam is affected by several different parameters such as media composition, cell surface properties of the microbe, surface-active proteins, and further metabolites of the microbe (Delvigne & Lecomte, 2009; Junker, 2007; Vardar-Sukan, 1992). Due to the strong surface-active properties of biosurfactants like rhamnolipids (RLs), foaming increases extensively and even small bubbles form persistent foam. In consequence, a phenomenon called *foaming out*

can be observed: microorganisms and the fermentation broth containing the nitrogen and carbon sources are discharged by foam bubbles. This reduces the biomass in the reactor and causes product loss (Anic et al., 2018). The foam can be used for product recovery, in a so-called foam fractionation approach, increasing however the unit operations like mechanical foam destroyer (Hoeks et al., 1997) or adsorption columns (Blesken et al., 2020). Alternatively, the application of antifoam detergents is widespread. However, these antifoam detergents require an additional effort in the downstream product purification, which leads to increased costs (Kosaric & Sukan, 2014). Membranes are a technical remedy for the reported obstacles because they enable bubble-free aeration of bioreactors (Coutte et al., 2010). In this study, we report a methodology of (a) designing a digital twin bioreactor incorporating novel architectures of membrane-aeration bundles, (b) rapid prototyping of a real-world membrane-aeration module, and (c) demonstrating improved fermentation productivity of biosurfactants using the prototypes.

1.1 | Membrane-aerated bioreactor

Today, bubble-free membrane-aeration finds application in two technical settings: While membrane-aerated biofilm reactors (MABfRs) are employed in waste-water treatment (Xiao et al., 2019), membrane-aerated bioreactors (MBRs) can be found in cell culture applications (Charcosset, 2012). In the former approach, biofilm growth on the membrane is desired, in the latter it is not. MABfRs and MBRs are very rare in industrial biotechnology (Cutayar et al., 1990; de Kronemberger et al., 2007). Their application is limited by the high oxygen demand of aerobic bacteria and yeasts in comparison to immobilized activated sludge on a membrane or suspensions of mammalian cell cultures.

Advantages of membrane-aeration are:

- prevention of foam formation (Coutte et al., 2010; de Kronemberger et al., 2007),
- high oxygen supply and energy efficiency (Syron & Casey, 2008),
- linear process scale-up by numbering-up of membrane area (Cote et al., 1988; Drioli et al., 2005),
- total shear stress reduction as no bubbles flow past the microorganism (Henzler, 2000), and
- mitigation of volatile organic compounds evaporation (Cote et al., 1988).

A challenge in MBR usage is the potential formation of an undesired biofilm on the membrane surface. This physical barrier essentially reduces the mass transfer performance and necessitates frequent and extensive cleaning or expensive modifications of the utilized membranes (Krishnan et al., 2008). Biofilm formation can be minimized by measures of process design (Carstensen et al., 2013) and module design (Deng et al., 2016), or avoided by genetic modification of the utilized microorganism (Gjermansen et al., 2010) and, in the case of biosurfactants, by the product itself (Irie et al., 2005).

Membrane-aeration in biosurfactant production fermentation has already been shown previously: de Kronemberger et al. (2007) produced RL by utilizing an external membrane-aeration module with *Pseudomonas aeruginosa* with glycerol as carbon source. A productivity of 30 mg L^{-1} h^{-1} RL was reported after 7 days of fermentation. The final concentration was approximately 6 g L^{-1} RL. Coutte et al. (2010) performed membrane aeration with two different external modules and one submerged membrane contactor in 3 L bioreactors (sMBR). During the fermentation of *Bacillus subtilis*, a productivity of maximum 3.2 mg L^{-1} h^{-1} surfactin (by external aeration) and 4.4 mg L^{-1} h^{-1} fengymcyin (by submerged aeration) was achieved. The studies by de Kronemberger et al. (2007) and Coutte et al. (2010) have in common that the utilized membrane module was either in an external loop (external membrane module approaches) or not designed for the specific reactor and stirrer configuration. A design approach that directly targets the mitigation of the boundary layer via the flow over the membrane will significantly influence the overall oxygen transfer (Cote et al., 1988, 1989) and consequently biomass and product formation.

1.2 | Bioreactors in CFD simulations

Mathematical models can help to understand the mass transfer characteristics of the above-mentioned sophisticated sMBR designs. In bioreactor technology, empirical models have been successfully developed and applied, where the process parameters are correlated to process variables under defined conditions (Nienow, 1998). Despite the benefits these empirical models provide, they are often based on a fixed and standardized geometry and are thus limited in their applicability.

Models based on computational fluid dynamics (CFDs) enable to identify and predict the process parameters and can be applied to various reactor designs. Additionally, the local conditions in the reactor are resolved instead of the global conditions (empirical models). Thus, the fluid flow is elucidated in detail and local mass transfer limitations can be detected (Bach et al., 2017).

The combination of CFD simulations in bioreactors with submerged membrane modules has been investigated by few researchers so far (Trad et al., 2015; Vlaev et al., 2018; Wu et al., 2018). Trad et al. (2015) focused on a system with an at-line membrane module for CO_2 perfusion and the optimization of mixing conditions in the reactor regarding the stirrer arrangement and geometry.

Vlaev et al. (2018) examined the flow characteristics in a stirred submerged membrane bioreactor (sMBR) with an inline tubular membrane module for an integrated production and recovery process. The biofouling behavior was evaluated by determining the shear rates at the membrane surface and the power input of the stirrers (Vlaev et al., 2018). Wu et al. (2018) investigated the effects of the membrane unit location in a full-scale membrane bioreactor on the hydrodynamic and the fouling behavior using CFD. The continuous phase was modeled with the standard k-epsilon turbulence model and the membrane unit was represented by a porous domain since the resolution of individual

membrane fibers was identified as too computationally costly. The fouling potential was studied using the liquid velocities at the boundary layer near the membrane surface, as the velocity is inversely related to the fouling rate: Regions with low velocities have a higher fouling potential. By comparing the velocity fields of different module locations, the fouling cannot be quantified, but different module locations can be compared qualitatively. In this study, the before mentioned CFD in situ membrane module bioreactor simulation approaches (Vlaev et al., 2018; Wu et al., 2018) are adjusted to fit the geometrically more complex objects here. We utilize this customized approach to optimize the design of the modules.

1.3 | RL produced by *Pseudomonas putida*

In addition to the fluid-mechanical process parameters, the microorganism has a strong impact on the process. Thus, the selection of a suitable microorganism as a biocatalyst for the production of a target molecule is crucial for the process performance. RL is industrially available biosurfactants of the class of glycolipids that have various potential applications in the cosmetic, food, and agricultural industries (De Almeida et al., 2016). Bubble-free membrane aeration would be an interesting technique for RL production, as even low concentrations induce excessive foaming (Demling et al., 2020; Gruber, 1991). In contrast to petroleum-based surfactants, RL are environmentally friendly (Banat et al., 2000), because they can be easily degraded by naturally occurring environmental microorganisms (Chong & Li, 2017; Soltani Dashtbozorg et al., 2016). They also prevent the formation of biofilms by weakening its structure (Davey et al., 2003). The natural RL producer *P. aeruginosa* is an opportunistic human pathogen entailing a complex regulation, which limits industrial application (Gunther et al., 2005). To overcome this restriction, the safety-level-1-organism *P. putida* KT2440, which is an industrially relevant microorganism, was genetically modified to produce RL by introducing two required genes from *P. aeruginosa* (Tiso et al., 2015, 2017; Wittgens et al., 2011). RL production from hydrophilic substrates like glucose or xylose with *P. putida* was shown before (Bator et al., 2020; Tiso et al., 2020), drastically improving the downstream process in contrast to hydrophobic substrates like plant oils, which are often used for RL synthesis by *P. aeruginosa* (Wittgens et al., 2011). As RL are excellent emulsifiers for oils, the product purification in presence of hydrophobic/oily substrates is elaborate and expensive (Müller et al., 2010).

In this study, we aim to produce RL from *P. putida* in a sMBR via bubble-free membrane aeration. In a first step, we design and rapid prototype membrane modules with different geometrical arrangements of the hollow fibers. These modules are investigated experimentally and via CFD simulations for their flow distribution. Subsequently, the more promising module approach is machined from reusable sterilizable materials and tested in (fed-) batch cultivations. Finally, we give an outlook to an advanced sMBR with an optimized geometric arrangement.

2 | MATERIALS AND METHODS

2.1 | Experimental set-up and fermentation procedures

The bioreactor was a 3 L glass vessel (Eppendorf) with a maximum filling volume of 2.3 L. The process was regulated by a control unit (BioFlo 120™) and DASware control software (v 5.3.1) (both Eppendorf). Fermentations were performed using mineral salts medium based on Hartmans et al. (1989). The common glucose concentration was 12 g L^{-1}. The fermentation temperature was controlled at 30°C. The bioreactors equipment, the detailed description of the process set-up and the sterilization procedure are presented in the Supporting Information Section 1.1.

The dissolved oxygen (DO) was controlled via the gas mixture, the transmembrane pressure (TMP), and the flow rate are specified in the respective section. Aeration was performed with synthetic air, pure oxygen, and mixtures of these gases (compare Section 2.2).

The oxygen transfer rate (OTR) was estimated via Henrys law and the DO concentration. Calculations are described in the Supporting Information Section 1.1.2. For fermentation, the reactor was inoculated with cells from a preculture to a final optical density (OD_{600}) of 0.5. The preculture was performed in 500 ml shake flasks with 10% filling volume at 30°C and 300 rpm with a throw of 50 mm. The medium had a threefold buffer capacity to counteract a decrease of pH due to gluconate production. In the fed-batch experiment, an automated DO-based feeding ensured nutrient supply after the batch phase.

2.2 | Aeration scheme

Two different aeration methods were used: cross-flow (CF) and dead-end (DE). During CF aeration, the air flows along the membrane fibers and is subsequently vented to the ambient air. The integrated DO cascade started aeration with 0 vol% O_2 and increased the O_2 content when the DO reached a certain threshold (here 20%). After an O_2 content of 100 vol% was reached, more O_2 could be supplied into the culture broth by manually increasing the TMP via the pressure regulator from the initial TMP of 0.3 bar up to 0.4 bar. While the O_2 content for the CF could be automatically controlled by the gas flow regulation of the control unit, the DE aeration started with 100 vol% O_2 but the gas flow was not constant.

The active flow was set to be 0.1 vvm. The O_2 flow was automatically adjusted when DO thresholds were reached: If the O_2 content in the liquid was below the threshold of 15%, the flow rate of O_2 was increased. When a concentration of 70% O_2 was reached, the airflow stopped to prevent an O_2 excess in the culture broth. The DO sensor (VisFerm DO ECS 225; Hamilton) was calibrated with pure oxygen to display the correct DO during cultivation. The TMP reached 0.4 bar during the active gassing phase and decreased during the off phase in which the O_2 was consumed. The initial oxygen concentration in the fermentation broth was set to 40% right before

the cultivation, to prevent oxidative stress or a delay of the anaplerosis by a low CO_2 concentration.

2.3 | Chemicals

In this study, bacteriological grade chemicals from Carl Roth GmbH & Co. KG, Merck KGaA, and Sigma-Aldrich Chemie GmbH were used. For analytic methods of RL- and sugar concentrations, analytical grade chemicals were used.

2.4 | Microorganisms

The bacterial strain *P. putida* KT2440 (DSM6125, ATCC47054) was described by other authors (Bagdasarian et al., 1981; Nelson et al., 2002). The engineered *P. putida* KT2440 SK4 harboring the RL genes from *P. aeruginosa* was used for heterologous RL production (Tiso et al., 2020).

2.5 | Biosurfactant and sugar quantification

RL quantification was performed similarly to a previously published method (Behrens et al., 2016). In brief, a reversed-phase chromatography (C18 column) coupled to a corona charged aerosol detector was used. The detailed procedure was described by Bator et al. (2020). To quantify the concentrations of D-glucose, D-gluconate, and 2-keto-D-gluconate, samples from the reactor were analyzed by high-performance liquid chromatography (HPLC). The detailed HPLC method was presented in Tiso et al. (2020).

2.6 | CFD simulations to optimize the module design

In this study, CFD simulations were performed with COMSOL Multiphysics 5.4. The geometry was designed in Inventor Professional 2019 (Autodesk) and imported as computer-aided design (CAD) file. Reactor components without function or influence on the fermentation, such as fillets and mounting chamfers, were removed from the CAD model to reduce the discretization effort. Material data of the bulk material *water* was taken from the COMSOL material library. The temperature was set to 30°C. The ambient pressure was kept constant. The model was defined with a pressure point constraint at a point at the top of the bioreactor that was set to 1 atm.

Here, both stationary and time-dependent solutions were investigated. The stationary simulation of the rotating parts in the bioreactor was implemented by the Multiple Reference Frame Model. The *frozen rotor* study separated the bioreactor into two different frames: A rotational frame around the moving agitator and a frame around the stationary parts, such as probes or membrane modules. The rotation of the rotational frame was solved using the Navier–Stokes equations with additional terms for Coriolis force and centrifugal force. The stationary solution was defined for one specific agitator position providing a solution for a pseudo-steady state.

The time-dependent simulation used the Sliding Mesh Model, which included a rotational frame and a stationary frame. The rotational speed of the rotational frame was set to $300\,s^{-1}$ (clockwise rotation). The time steps were chosen to be $0.01\,s^{-1}$ to obtain a rotation by 18° for each time step and thus to avoid convergence errors.

The implementation of the membrane reactor showed that a turbulence model is most suitable. The fluid flow simulations were performed with the "Rotating Machinery, Turbulent Flow, k-epsilon interface" from COMSOL. It is suitable for incompressible single-phase flow with high Reynolds numbers and for geometries with rotating parts, such as the agitator in the bioreactor. A pre-examination showed a justified reduction from three-dimensional (3D) to 2D to investigate certain aspects.

Agglomeration of particles on the membrane can cause biofouling. Additionally, high concentrations of dissolved gases can cause outgassing or bubble formation. Thus, all simulations were evaluated regarding the following parameters:

(1) average shear rate at the membrane surface $\dot{\gamma}_B$,
(2) average fluid velocity in the bioreactor $\bar{v}_{Total}$.

Regarding (1), the average shear rate at the membrane surface $\dot{\gamma}_B$ is a measure for the incident flow to the membrane. A high shear rate implies a high mass transport of substances into the medium through the membrane (in this case DO). Besides, the agglomeration potential of substances at the membrane surface is smaller for high induced shear rates.

Regarding (2), the average fluid velocity in the bioreactor $\bar{v}_{Total}$ should be high when comparing the investigated bioreactor geometries to avoid regions with low velocity. Those dead zones hamper the supply with nutrients and oxygen and diminish the overall process performance of the bioreactor.

A mesh independence study was performed for the geometry of the bioreactor including internals and an agitator with two Rushton turbines but without the membrane (see Supporting Information Section 2.2.1). The shear rates $\dot{\gamma}$ at the stirrers surface and at the reactor wall were investigated as a function of the mesh elements. To mesh the geometry, unstructured meshes, geometry partitioning, and swept meshes were used.

The hollow fiber membranes of the bioreactor demand further complexity reduction as they are only a few micrometers thick and thus orders of magnitude smaller than the dimensions of the 3-L reactor.

Preliminary simulations of the membrane abstraction as a closed wall, as individual fibers, as a screen boundary condition and as porous domain were compared for a single blade and various incident angles Φ (see Supporting Information Section 2.2.5) As a result, the membrane lamellae were modeled as closed wall, since the representation as hollow fiber meshes cannot be efficiently simulated in terms of time and computational resources. In addition, experimental investigations showed that flow between the individual hollow fibers is negligible.

The blade angle and size of the membrane blades strongly influence intermixing in the bioreactor. Φ Refers to the angle between the tangent of a circle through the center of the blades and the blade itself. The following angles were investigated: $\Phi = 0°$, 12.5°, 22.5°, 32.5°, and 82.5°. Blade angle $\Phi = 0°$ corresponds to the Pillar module and $\Phi = 22.5°$ corresponds to the prototyped Vortex module. Inner and outer diameter and the height of the membrane module were kept constant. Due to fabrication issues, a minimum gap distance of 2 mm between the blades was implemented. The blade width, the total number of blades and thus the number of hollow fibers per blade was adapted to Φ. Since an increasing number of hollow fibers creates a larger contact surface for the oxygen supply, a high amount of fibers is preferable.

The stationary solution of the *frozen rotor* approach depends on the position of the agitator relative to the stationary parts. As the agitator position repeats every 60°, the simulated agitator position is changed in 20° steps. The R1 agitator configuration (see Supporting Information Section 2.2.4) is used, as it shows promising results regarding the process performance in previous works and in the investigation of the agitator configuration.

Regarding the agitator configuration, different stirrer types (radial stirring Rushton turbine, axial radial stirring Pitched Blade Turbine), the number of stirrers (2–4), and the stirrer distances in both the empty reactor and including the Vortex module were investigated (see Supporting Information Section 2.2.4).

2.6.1 | Test-module conceptualization

The test modules were designed with regard to the geometric constraints of the bioreactor compartment. More information about the dimensional survey of the bioreactor and the fabrication of the test modules are shown in Supporting Information Section 1.2.

Two design variations were investigated: (a) In the first approach, a membrane mesh was arranged in a circular configuration around the stirrer (*Pillar* type). (b) In the *Vortex* approach, the membrane mesh was sliced into short lamellae, which were arranged as blades in a circular arrangement in flow direction around the stirrer.

This conceptualization process is presented in Figure 1. Further details on the membrane modules, such as resuming membrane area, can be found in Supporting Information Section 1.3. The integrated test modules were compared by measuring the DO in 30°C warm water. The stirrer configuration was chosen as described in Supporting Information Section 1.1.1.

2.6.2 | Construction of the metal vortex module prototype

A robust Vortex module prototype machined from stainless steel was used for the fermentation. The design and material selection were performed under consideration of the special demands of a bioprocess like sterilization, biocompatibility, and mitigation of dead zones for anti-fouling properties. Further information about the prototype fabrication and assembly are given in Supporting Information Section 1.3. The final Vortex module and its components are presented in Figure 2a.

3 | RESULTS AND DISCUSSION

Based on the bioreactor's digital twin, CFD studies were evaluated with the aim to find a membrane module design with customized flow conditions. Here, we show the CFD results of a comparison of two different module types. Hereinafter, we present the mentioned

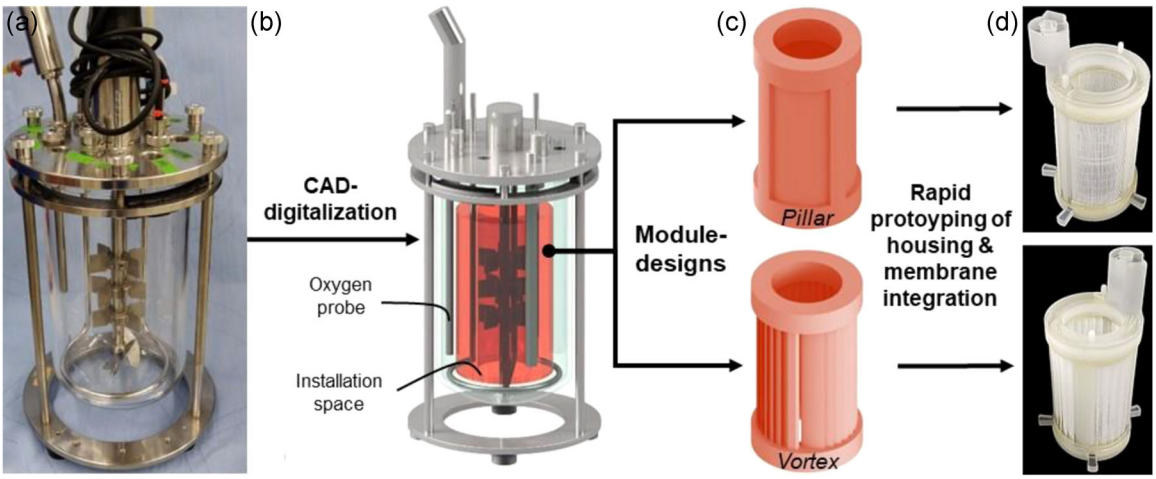

FIGURE 1 Rapid prototyping fabrication scheme for tailor-made submerged membrane-aeration modules: (a) 3-L bioreactor including stirrer configuration, probes, and cooling circuit; (b) *Digital Twin* of the bioreactor with free installation space (highlighted in red) and position of the oxygen probe; (c) two different designs of membrane test modules derived from the free installation volume: The simple-to-build Pillar module and the Vortex module with several membrane-mesh compartments and increased membrane area; (d) ready-to-use test-modules for estimation of oxygen transfer in the bioreactor. CAD, computer-aided design

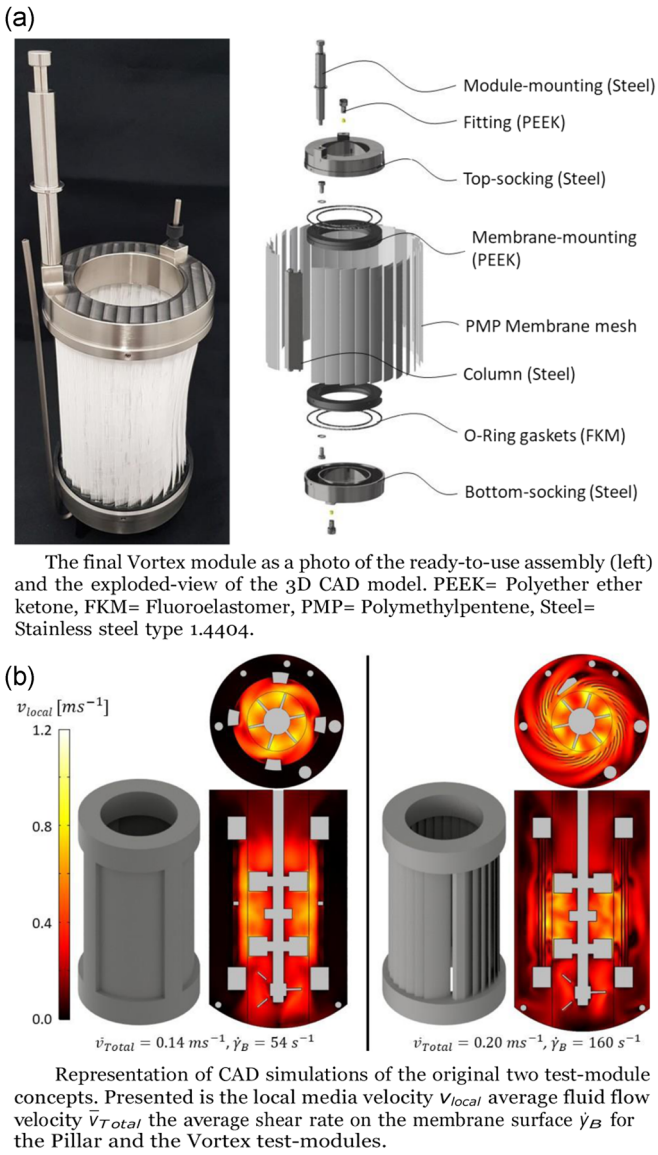

The final Vortex module as a photo of the ready-to-use assembly (left) and the exploded-view of the 3D CAD model. PEEK= Polyether ether ketone, FKM= Fluoroelastomer, PMP= Polymethylpentene, Steel= Stainless steel type 1.4404.

Representation of CAD simulations of the original two test-module concepts. Presented is the local media velocity v_{local} average fluid flow velocity $\bar{v}_{Total}$ the average shear rate on the membrane surface $\dot{\gamma}_B$ for the Pillar and the Vortex test-modules.

FIGURE 2 Milestones of the membrane module evolution: (a) the construction of the final Vortex module; (b) the digital comparison of the initial design approaches. CAD, computer-aided design

oxygen transfer results of the test-module evaluation of the two design approaches. As the superiority of the Vortex approach is supported by CFD and test-module evaluation, a prototype was manufactured and representative fermentations were performed. A comparison of the fermentation results and a thereupon-based design optimization study finalizes this section.

3.1 | CFD comparison of pillar and vortex module

CFD simulations enabled a comparison of the digital twin of the Pillar module and the Vortex module. Figure 2b shows a CAD sketch and the resulting 3D simulation of the two modules. The simulation images show the velocity in 2D plots of a vertical and a horizontal cross-section. The flow distribution in the bioreactor with the Pillar module shows large gradients of the flow velocity. The outer regions show significant large areas of velocities below 0.2 m s^{-1} (in black) and a velocity reduction of about 80%. The Pillar module contains one single membrane blade, which impedes flow through the membrane to the outer regions. It must be considered, that the membrane blade, which in reality consists of multiple hollow fibers, is modeled as a closed wall without permeability in this study (see Section 2.6). Experimental investigations with rapid-prototyped modules showed that this assumption agrees with reality (see Section 3.2).

The lamellar construction of the Vortex module enables flow into outer bioreactor regions. In contrast to the Pillar module, this configuration results in a more homogeneous velocity distribution with about 50% difference between the inner and the outer velocity profiles. Larger flow-impeded zones are only detected behind the probes and the module support column. An induced vertical loop flow distributes the medium from the bioreactor center along with the membrane blades and through the outer bioreactor region to the

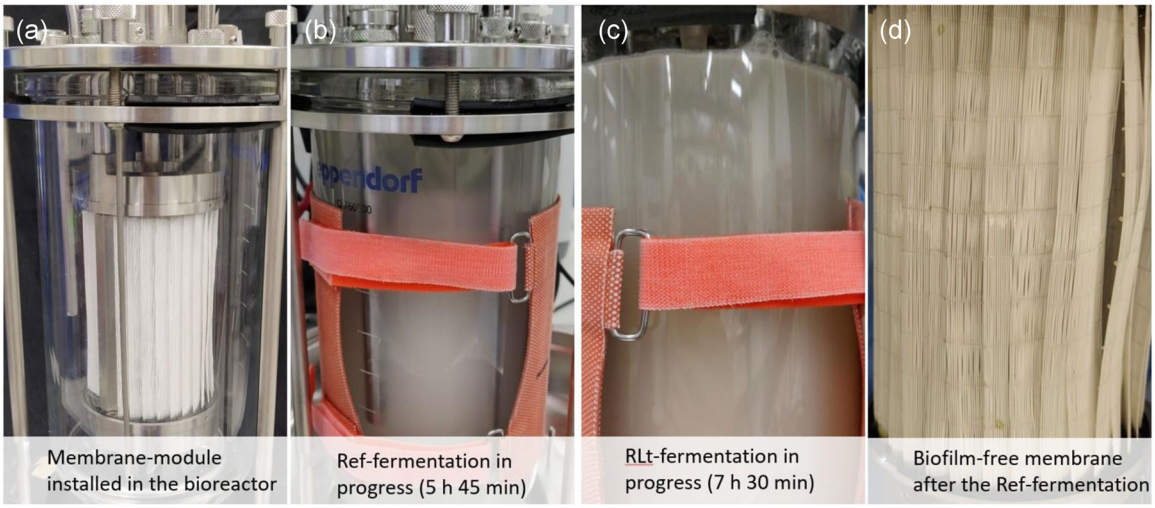

FIGURE 3 The Vortex prototype during the processes: (a) Inside the bioreactor with the installed probes, stirrer, and cooling circuit before filling the reactor. (b) The bioreactor after 5 h 45 min of the wild-type strain fermentation (ref) showing increasing turbidity of the media ($OD_{600} \approx 4$). (c) The rhamnolipid (RL) production fermentation (Batch 2, cross-flow [CF]) directly before reaching the highest OD_{600} (9) after 7 h 30 min without foaming. (d) Picture of the membrane mesh directly after the ref-fermentation. (a) Ref-fermentation with CF aeration mode. The fermentation was conducted with 8 g L^{-1} glucose, initial gas feed = 100 vol% air and a DO control to increase O_2 content in gas up to 100 vol%. Further settings: Gas flow = 1 vvm, TMP = 0.3–0.35 bar, OD_{600} after inoculation = 0.2; V = 2.3 L. (b) RL-fermentation with CF aeration mode (Batch 2, CF). The fermentation was conducted with 11.98 g L^{-1} glucose, initial gas = 100 vol% air, DO control to increase O_2 content in gas up to 100 vol% if DO < 15%, gas flow = 1 vvm, TMP = 0.3–0.4 bar. (c) RL-fermentation with dead-end (DE) aeration mode (Batch 3, DE). The fermentation was conducted with 12.17 g L^{-1} glucose, initial gas = 100 vol % O_2, DO control to add O_2 while DO < 15% until DO > 70%, gas flow = 0–0.1 vvm, TMP = 0–0.4 bar. (d) RL-fed-batch fermentation with DE aeration mode (fed-batch, DE). The fermentation was initially conducted with 13.28 g L^{-1} glucose, gas = 100 vol% O_2, DO control to pump O_2 while DO < 15% until DO > 70%, gas flow = 0–0.1 vvm, TMP = 0–0.4 bar, glucose fed: 750 g L^{-1}. Via the fed-phase 20 g glucose was added. DO, dissolved oxygen; OD, optical density; TMP, transmembrane pressure

bottom and top of the bioreactor; and back to the module center. The average fluid flow velocity $\bar{v}_{Total}$ as well as the average shear rate on the membrane surface $\dot{\gamma}_B$ show higher values for the Vortex module compared to the Pillar module. The low values of $\dot{\gamma}_B$ for the Pillar module can be explained by the low velocities at the membrane's backside. This results in an increased potential for biofouling and outgassing, where the latter is also observed in experiments (see Section 3.2). As the simulation results suggest superiority of the Vortex module, fast prototyping was utilized to fabricate test modules (see Section 2.6) to prove the CFD results.

3.2 | Preliminary test-module evaluation

Results of the abiotic oxygen transfer measurements with synthetic air and oxygen are presented here. Even though the selected method for gas feeding is close to the later application, the sensitivity of the method is arguable but feasible for a direct and fast comparison of different modules. With synthetic air, test modules showed a corrected maximal OTR of 3.9 mmol L^{-1} h^{-1} (Pillar) and 5.7 mmol L^{-1} h^{-1} (Vortex). With O_2, the modules showed a corrected maximal OTR of 26.9 mmol L^{-1} h^{-1} (Pillar) and 55.0 mmol L^{-1} h^{-1} (Vortex). Thus, the Vortex test module induces a higher oxygen transfer. Presented data are corrected for the influence of the oxygen entry via the fermenters head by −0.1 mmol L^{-1} h^{-1} (empirical determined value). Graphs of the OTR determination are presented in Supporting Information Section 2.1. During the DO measurement, we observed frequent bubble formation at the outer membrane shell side of the Pillar test module. In comparison to the Vortex test module, the fluid outside the membrane perimeter was significantly less mixed in the Pillar test module, as modeled by the simulation results in Figure 2b. Also, bubble formation on the membrane occurred sparsely in the Vortex arrangement at higher DO. The approximation of the simulated impermeable membrane wall was thereby confirmed. This flow barrier favors concentration polarization on the outer shell side of the membrane, which leads to the bubble formation at the Pillar test module. As the oxygen transfer and mixing of the Vortex test module prototype was superior to the Pillar test module prototype, the Vortex approach was chosen for the fermentation experiments.

3.3 | Fermentation processes with the vortex prototype

3.3.1 | Reference-benchmark fermentation

In a first step, the oxygen transfer and the growth pattern of *P. putida* reference (ref) without the RL production genes was investigated.

The experiment was conducted with the default parameters for the *CF* process described in Section 2.1 and ran for 9.5 h. Photographs of the Vortex prototype in the bioreactor before and during the ref-fermentation are shown in Figure 3.

Figure 4a presents the OD_{600}, the DO and glucose concentration during the fermentation. The DO started at 100% and steadily decreased over the first three hours. This decrease is associated with the increasing O_2 demand caused by the microbe's growth. After 3.5 h, the DO concentration fell below the set threshold of 20%, which triggered the aeration cascade to supply O_2 to the culture. The concentration of O_2 in the inlet gas flow was increased steadily to boost the mass transfer between gas and liquid (see Supporting Information Section 1.1.3). The ratio of oxygen to synthetic air was automatically increased by the controller to keep the DO above 20% in the solution. The two DO spikes after 5 and 7 h are due to manual adjustments of the TMP to increase the O_2 transfer. After 7 h, the inlet gas flow consisted of 100 vol% O_2. Because of the last adjustment of the gas regulation, the TMP increased to 350 mbar. This led to an increased O_2 transfer over the membrane and the O_2 content in the gas was automatically reduced to 80 vol% by the controller.

The final peak after 9 h marked the end of the fermentation, as all glucose was consumed. Because the O_2 was not consumed

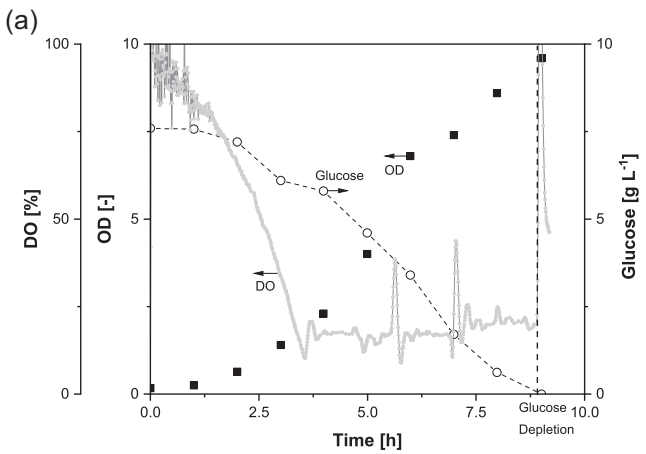

Ref-fermentation with cross-flow aeration mode. The fermentation was conducted with 8 g L^{-1} glucose, initial gas feed = 100 vol% air and a DO control to increase O_2 content in gas up to 100 vol%. Further settings: Gas flow = 1 vvm, TMP = 0.3 to 0.35 bar, OD_{600} after inoculation = 0.2; V=2.3 liter.

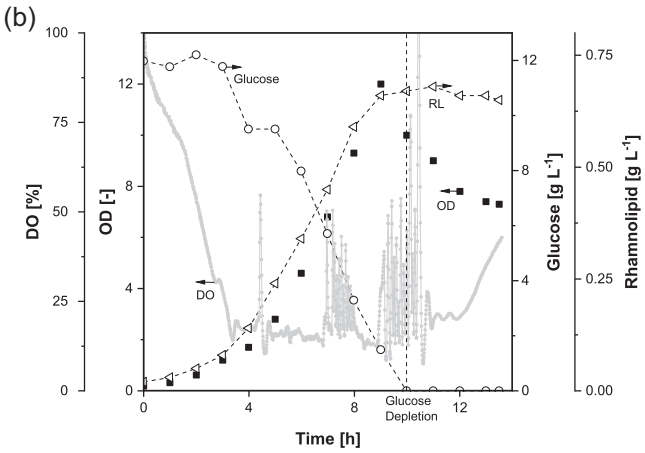

RL-fermentation with cross-flow aeration mode (batch 1 (CF)). The fermentation was conducted with 11.98 g L^{-1} glucose, initial gas = 100 vol% air, DO control to increase O_2 content in gas up to 100 vol% if DO < 15 %, gas flow = 1 vvm, TMP = 0.3 to 0.4 bar.

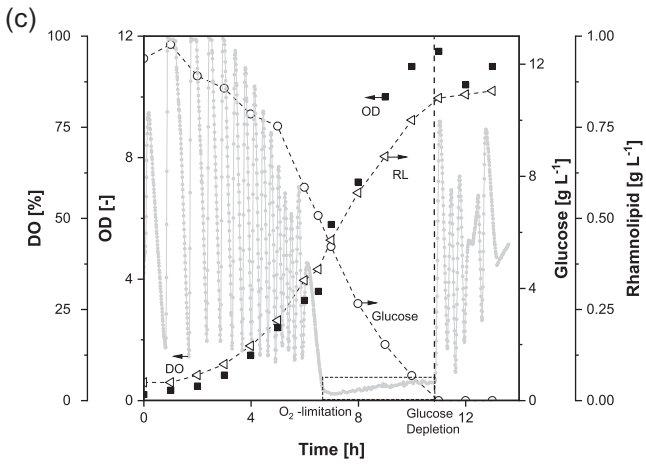

RL-fermentation with dead-end aeration mode (batch 3 (DE)). The fermentation was conducted with 12.17 g L^{-1} glucose, initial gas = 100 vol % O_2, DO control to add O_2 while DO < 15 % until DO > 70 %, gas flow = 0 to 0.1 vvm, TMP = 0 to 0.4 bar.

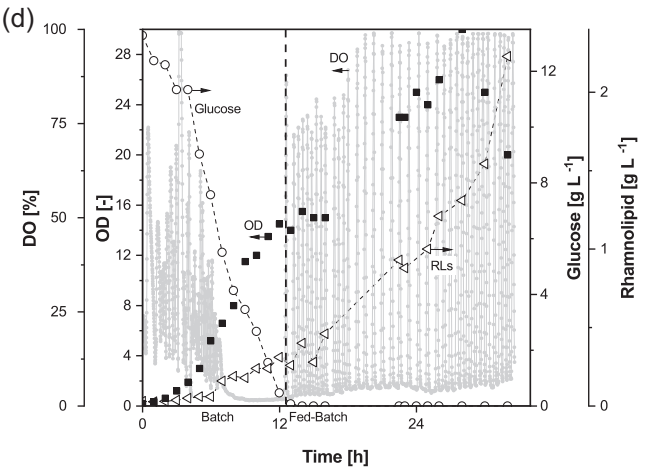

RL-fed-batch fermentation with dead-end aeration mode (fed-batch (DE)). The fermentation was initially conducted with 13.28 g L^{-1} glucose, gas = 100 vol% O_2, DO control to pump O_2 while DO < 15 % until DO > 70 %, gas flow = 0 to 0.1 vvm, TMP = 0 to 0.4 bar, glucose fed: 750 g L^{-1}. Via the fed-phase 20 g glucose where added.

FIGURE 4 Results of four different fermentations performed with the Vortex prototype. All used mineral salts medium (according to Hartmans et al., 1989), *N* = 300 rpm; *T* = 30°C; pH = 7. For further fermentation, information compare Section 2.1. CF, cross-flow; DE, dead-end; DO, dissolved oxygen; OD, optical density; RL, rhamnolipid; TMP, transmembrane pressure

anymore, the O_2 concentration rose. The OD_{600} was initially at 0.2, as described in Section 2.1. Exponential growth was observed until 6 h. After 6 h, a linear growth was observed. A final OD_{600} of 9.6 was reached with a maximal growth rate of 0.46 h^{-1}.

The initial glucose concentration was measured to be 8 g L^{-1}. With increasing biomass concentration an increased glucose depletion was observed. After 9 h, no glucose could be detected within the culture broth, which aligns with the above described DO peak after nine hours. After the removal of the module from the reactor, no macroscopic biofouling was observed. Additionally, no gas leaks were observed. Thus, the system presented herein can be used to conduct bubble-free fermentations over a defined period of time.

3.3.2 | RL production batch fermentation with CF aeration

Pictures of the installation of the Vortex module before and during the RL fermentation are shown in Figure 3. The results of the fermentation are shown in Figure 4b.

After the benchmark fermentation with the wild-type strain, the recombinant strain *P. putida* KT2440 SK4 was cultivated for around 10–15 h in duplicate (see Figure S7). The evolution of the DO was similar to the benchmark fermentation in Section 3.3.1. In contrast to the duplicate CF fermentation (compare Supporting Information Section 2.3), more O_2 could be supplied in the first run after the TMP was increased to 0.4 bar because the control unit did not reduce the gas flow. The manual adjustment of the TMP caused oscillation of the DO signal between 9 and 10.5 h. The DO was always above 10%. Therefore, an oxygen limitation can be excluded.

The glucose concentration started at 12 g L^{-1} and decreased inverse proportionally to the biomass concentration. Glucose was depleted after 10 h, which can also be seen in the DO signal above 75% at this point in time. Glucose depletion was marked with a dashed line in the diagram. Due to the oscillating DO signal, the peak was not as clear as in the previous fermentation. The fermentation was extended until a DO of 40% was reached. No lag-phase was observed in both CF experiments. A maximal growth rate of 0.51 h^{-1} was observed, which is in the same range as the duplicate and the ref-fermentation. Initially, the culture showed an exponential growth phase, which slowed down to a linear growth during the oxygen limitation (4.5–11.5 h). The biomass increased until the glucose was depleted (11.5 h) and reached a maximal OD_{600} of 12, which corresponds to a biomass concentration of 3.7 g L^{-1}. The RL concentration followed the biomass closely until the stationary phase was reached. The more biomass is present in the culture, the more RL is produced. After glucose depletion was reached, the RL production stopped as well. A final RL titer of 680 mg L^{-1} was achieved. The produced amount of RL is around 20% lower than in the duplicate. There was no oxygen limitation in this fermentation, which is suspected in duplicate Batch 2 (CF). As *P. putida* is known for its flexible redox system. We thus hypothesize that RL could act as an electron acceptor under anaerobic conditions. Since *P. putida* probably produces more RL during an oxygen limitation, less RL was produced in the first run and the carbon source was converted to biomass (Gruber et al., 1993). As in the reference/wild-type fermentation, neither biofouling on the membrane was observed nor foam formation.

3.3.3 | RL production batch fermentation with DE aeration

As an alternative to the CF fermentation, the aeration mode was switched to DE. Therefore, the module outlet is closed during DE aeration, which traps the gas in the module. The DE aeration can potentially be more efficient in terms of oxygen conversion. CO_2 can only be discharged through the fermenter head and the outlet via the condenser or short (CF) flushings of the module inside. Here, CO_2 was removed via the fermenter head. The fermentation lasted 13 h. The glucose and RL concentrations, as well as the OD_{600} and DO are shown in Figure 4c. The DO started at 40% to avoid initial oxidative stress (Gruber et al., 1993) and anaplerosis delay. High oxygen concentrations at the membrane-shell side can additionally lead to concentration polarization and bubble formation. These microscopic bubbles can lead to an extraction of CO_2, because the concentration gradient between bubble and broth is high. Nevertheless, the oxygen content reached 100% several times during the start of the fermentation due to imprecise regulation by the utilized controller. This may have led to a decreased growth rate due to oxidative stress (Alagappan & Cowan, 2004) or delay of the anaplerosis. The oscillating DO signal resulted from the gas flow being turned on and off until after 6.5 h a consumption rate was reached where the gas could be supplied continuously. The DE aeration had a lower OTR in comparison to the CF (compare Section 3.2) which led to an oxygen limitation between 6.5 and 10.5. The glucose concentration started at 12 g L^{-1} and was depleted after 11 h which led to a DO peak, as observed before. Afterward, the oxygen demand increased again. This resulted in a similar oscillation of the DO signal as seen in the first 6 h of the fermentation.

No lag-phase could be detected during the cultivation and a maximal growth rate of 0.4 h^{-1} was observed. The exponential growth phase lasted for 5 h until the culture became oxygen-limited. *P. putida* showed a linear growth under oxygen limitation. During this 4-h time frame, the OD_{600} increased from 3.3 to 11.0. The culture entered the stationary phase with the depletion of glucose and the OD_{600} decreased slowly. A maximal OD_{600} of 11.5 was reached and 40 L_{O2} was consumed. This was only 13.5% of the oxygen used for the CF fermentation, during which 300 L_{O2} was used. The RL concentration increased proportionally to the biomass concentration until the glucose was depleted and reached a final concentration of 860 mg L^{-1}. The production was slower than the RL production in the previous experiments, which is likely linked to the oxidative stress or a delay of the anaplerosis during the first hours.

However, the final RL concentration was similar. This is attributed to the longer oxygen limitation in the DE experiment, which lasted 4 h.

We hypothesize that *P. putida* produces proportionally more RL during an oxygen limitation because the growth is inhibited (Gruber et al., 1993), which led to the similar final titers for both the CF and DE processes.

3.3.4 | RL production fed-batch fermentation with DE aeration

To demonstrate the long-term stability of the module and maximize product concentration, fed-batch fermentation was performed. In contrast to the previous fermentations, the filling volume was reduced to 2.1 L to provide more volume for feeding. Otherwise, no modifications were made. The glucose feed had a concentration of 750 g L^{-1}. The main results of the fermentation are shown in Figure 4d. The initial batch phase lasted for 12 h. After that, the fed-batch phase was initiated by intermediate DO triggered feeding of glucose. The gassing script was slightly changed (compare Section 2.2 and Supporting Information Section 1.1.5) to reduce the gassing duration, which reduced the maximal oxygen content in the culture broth. This change in the script reduced the oxidative stress supposed in the previous experiment.

The gas flow was constant after 7 h and the process-controller-caused oxygen limitation because not enough oxygen could be supplied. This limitation lasted until 11.3 h, after which the glucose was fully consumed. The DO signal increased sharply because the organisms alter their metabolism due to the lack of glucose. After the DO signal reached 40%, the feeding script started, and additional glucose was supplied. The bacteria started to metabolize the glucose again and the DO signal decreased until the glucose was depleted once more, which started the cycle again. This led to an oscillating DO signal. Each peak lasted approximately 30 min, but the duration decreased with increasing biomass. The initial glucose concentration was 13 g L^{-1}. Twenty grams of glucose were fed during the fed-batch phase, which resulted in theoretical glucose concentration of 33 g L^{-1}.

The OD_{600} showed no lag phase similar to the other experiments with the modified strain. Exponential growth was observed until an oxygen limitation after 7 h. During this phase, a maximal growth rate of 0.48 h^{-1} was observed. Biomass was produced at a faster rate in contrast to the previous DE experiment, which is likely connected to the adjusted O_2 concentration during the initial hours of the fermentation.

Due to the oxygen limitation, a linear growth occurred until the glucose was consumed after 10 h. No significant growth was observed during the first few hours of the fed-batch phase. To prevent a trace element limitation, 20 ml trace elements stock solution was added (compare Supporting Information Section 1.1.6). Growth was observed again until the OD_{600} peaked at 28 after 30 h. The OD_{600} decreased subsequently, presumably due to a depletion of nutrients like phosphate. The DO course for the first 14 h is similar to the previous DE fermentation. The initial oxygen content was adjusted to less than 100% just before the inoculation to prevent oxidative stress and an anaplerotic delay.

An exponential decrease in glucose could be seen during the first hours of cultivation, until the oxygen limitation (DO < 10%) came into effect after 6.5 h. After that, the course followed a linear decrease until it was depleted after 11.5 h. No glucose could be detected for the rest of the fermentation.

The initial RL production rate was lower in comparison to the previous cultivation, presumably because the organisms were less stressed or were able to perform anaplerotic reactions at the beginning of the cultivation. This led to an increased growth rate. Since more substrate was used for biomass production, less RL was produced during the first 13 h of the cultivation in comparison to the previous DE batch. The average RL production was 26 versus 77 mg L^{-1} h^{-1} for the previous DE batch experiment. This correlates with the different growth rates of the cultivations (precultivation and main fermentation) as well. During the fed-batch phase, an average RL production of 95 mg L^{-1} h^{-1} was achieved. This resulted in a final RL concentration of 2.2 g L^{-1}.

During the DE processes more bubbles formed at the membranes surface than during the CF aeration. This was caused by the intense pressure regulation peaks. During these peaks, bubbles could form at the membrane–liquid interphase (Cote et al., 1988). In combination with the increased organic matter in the culture broth, enough foam could form to *foam out* after 32 h. To prevent foam formation, the process should be conducted with a more precise gas controller. After the fermentation, no biofilm was observed on the membrane. This demonstrates that the membrane material and design are suitable even for long processes without causing leaks or visible biofouling.

3.3.5 | Comparison of the different fermentations

The most important results of the four fermentations are shown in Table 1. Due to the preparation of a calibration curve in the occurring OD_{600} range, a conversion factor of 1 OD_{600} ≈ 0.31 g_{BM} L^{-1} was estimated with six data points by an Ultrospec 10 cell density meter (Biochrom). A defined volume was filtrated through cellulose–nitrate filter and the filter was weighed before and after filtration and drying at 100°C. By comparison of the duplicated CF batches, the maximum RL concentration per initial glucose concentration differs about 94%. We explain this difference by the oxygen supply by the controller settings. In the duplicate CF batch (Batch 1), the exponential growth of biomass was probably oxygen-limited and became linear. The RL conversion was not affected by the oxygen concentration and was continuous. In contrast, glucose in Batch 2 is converted at higher rates to biomass. This diminishes free substrate for the RL production. Thus, there is a high potential for optimization of the glucose conversion in the fermentation of RL from *P. putida*: a sensitive control of the process aeration should be implemented for product

TABLE 1 Display of rhamnolipid (RL) production, yields of RL and biomass per glucose and oxygen, respectively, shown in batch and fed-batch fermentation

Fermentation process	t (h)	Final OD_{600} (OD_{600})	Final BM conc. (g L^{-1})	μ (h^{-1})	RI titer (g L^{-1})	STY (mg_{RL} L h^{-1})	RL/Glu (mg_{RL} g_{Glu}^{-1})	RL/O_2 (mg_{RL} L^{-1})	BM/O_2 (mg_{BM} L^{-1})	BM/Glu (g_{BM} g_{Glu}^{-1}
Batch 1 (CF)	13.5	12	3.7	0.51	0.68	67	57	2.3	29	0.71
Batch 2 (CF)	12.0	10.3	3.2	0.48	0.86	86	109	3.7	31	0.93
Batch 3 (DE)	13	11.5	3.6	0.40	0.85	77	70	20.9	202	0.67
Fed-batch (DE)	32	28.0	8.7	0.48	2.23	67	96	10.4	93	0.60

Note: With t, runtime; BM, biomass; μ, growth rate; STY, space–time yield until Glu depletion, CF, cross-flow, and DE, dead-end. Oxygen values are based on the extra oxygen input via cascade or DE aeration, only.

yield maximization. As assumed, the DE fermentations Batch 3 and the fed-batch showed the best RL to O_2 ratio. Up to seven times more RL per supplied oxygen was produced compared to the CF batches. This is even more pronounced in sight of the biomass to oxygen ratio but shows the versatile purpose opportunities for this kind of submerged membrane module. The fed-batch had the highest RL titer with 2.2 g L^{-1} but with the oxidative stress, caused by the oxygen control, the STY of Batch 1 was 24% higher. Compared to the external module approach of de Kronemberger et al. (2007), a higher STY for the production of RL was found. In our study, the STY was 2.3 (DE aeration) to 2.8 times (CF aeration) higher.

3.3.6 | Simulative optimization of the module design

As seen in Section 3.3.5, the Vortex module is feasible in most of the applied fermentation processes. Still, processes with a higher biomass concentration and thus higher demand in oxygen supply (e.g., by air-CF gassing) are desired to shorten the process time or reduce process operation costs. Besides fine-tuning the process control, geometric optimization of the module's architecture regarding packing density and flow distribution is another key factor in reducing mass transport limitations and achieving the best fermentation results. Including the presented 3D CFD simulation approach in

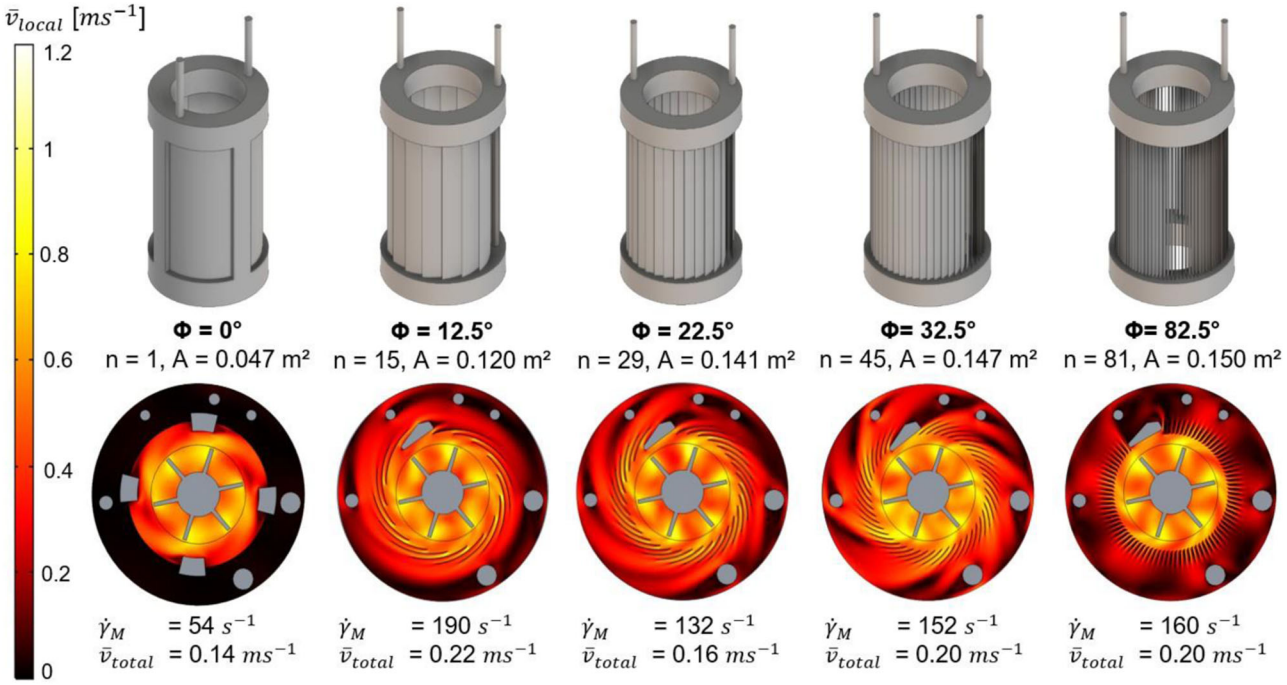

FIGURE 5 Comparison of different membrane module design with the local flow velocity v_{local}, average fluid flow velocity $\bar{v}_{Total}$ and average shear rate on the membrane surface $\dot{\gamma}_B$ for the Pillar module and Vortex modules with different membrane angles φ as well as the number of membrane meshes (n) and the calculated membrane area (A). (a) The final Vortex module as a photo of the ready-to-use assembly (left) and the exploded-view of the 3D CAD model. (b) Representation of CAD simulations of the original two test-module concepts. Presented is the local media velocity v_{local} average fluid flow velocity $\bar{v}_{Total}$ the average shear rate on the membrane surface $\dot{\gamma}_B$ for the Pillar and the Vortex test modules. 3D, three-dimensional; CAD, computer-aided design; FKM, fluoroelastomer; PEEK, polyether ether ketone; PMP, polymethylpentene; steel, stainless steel type 1.4404

Section 2.6, a perspective optimization approach was conducted aiming for the highest average fluid flow velocity $\bar{v}_{Total}$ and highest average shear rate on the membrane $\dot{\gamma}_B$, under the given physical and fabricating constrains. So far, the R1 agitator configuration was used, as it showed promising results regarding the process performance in previous investigations (see Supporting Information Section 2.2.4). Design optimization was performed for a varying membrane angle of incidence φ while making maximum use of the resulting membrane area. The simulation results are depicted in Figure 5.

Here, a membrane angle of incidence $\varphi = 0°$ complies with the Pillar module and $\varphi = 22.5°$ with the Vortex module. $\varphi = 12.5°$ and $\varphi = 32.5°$ are gradual variations of the Vortex module, completed by a membrane angle $\varphi = 82.5°$ representing orthogonal incident fluid flow on the membrane meshes. Low values for v_{local} at probes or mountings highly depend on the virtual rotary position of the agitator blade. By choosing a different rotational degree of the agitator position, results of those low-velocity zones vary significantly (data not shown) thus dead-zone formation can be excluded for all approaches $\varphi > 0°$. The $\varphi = 12.5°$ simulation shows the highest resulting $\bar{v}_{Total}$ and $\dot{\gamma}_B$. Despite the lower membrane surface (−15%), the influence of the higher $\dot{\gamma}_B$ (+30%) could compensate the loss in membrane area. A physical validation of this hypothesis has not yet been performed. Results of the CFD investigation show a region of an optimal membrane-mesh angle $\varphi = 22.5° \pm 10°$, depending on whether a large membrane area (smaller angle) or good mixing (larger angle) shall be achieved.

4 | CONCLUSION

We report a fast and universal design and manufacturing method for flow-optimized submerged membrane modules in bioreactors. The 3D-printed prototype is based on CFD simulations for mass transport optimization. It enables high oxygen transfer into the reactor and foam-free fermentations of RL-producing bacteria. The fermentation broth was aerated with air and pure oxygen in CF or DE mode and we demonstrate the superior oxygen supply of the latter, which reaches 20 $mg_{RL}\,L^{-1}$. Thus, we efficiently synthesized RL with an STY of 86 $mg_{RL}\,L\,h^{-1}$. The design approach of this study unleashes the potential of fermentation processes without foam formation, which is nowadays related by physicochemical or economical barriers.

ACKNOWLEDGMENTS

The scientific activities of the Bioeconomy Science Center were financially supported by the Ministry of Innovation, Science, and Research within the NRW Strategieprojekt BioSC (Grant No. 313/323-400-00213). Furthermore, the authors want to thank Christian Reich, Tobias Karmainski, Dominik Engel, Moritz Meyer, and Felix Stockmeier for their valuable input and many fruitful discussions. Simulations were performed with computing resources granted by RWTH Aachen University under project thes0610.

CONFLICT OF INTERESTS

The authors declare that there are no conflict of interests.

AUTHOR CONTRIBUTIONS

Patrick Bongartz: Conceptualization; data curation; investigation; methodology; writing – original draft; writing – review and editing; visualization; validation. **Isabel Bator**: Methodology; investigation; validation; resources; writing – review and editing. **Kristina Baitalow**: Methodology; investigation; validation; visualization; software; writing – review and editing. **Robert G. Keller**: Writing – review and editing; funding acquisition. **Till Tiso**: Methodology; validation; writing – review and editing; supervision; funding acquisition. **Lars M. Blank**: Methodology; validation; writing – review and editing; supervision; funding acquisition. **Matthias Wessling**: Conceptualization; writing – review and editing; supervision; funding acquisition; project administration.

DATA AVAILABILITY STATEMENT

The data that support the findings of this study are available from the corresponding author upon reasonable request.

ORCID

Patrick Bongartz https://orcid.org/0000-0002-2240-2671
Kristina Baitalow https://orcid.org/0000-0003-2336-8126
Robert Keller https://orcid.org/0000-0001-7053-0195
Till Tiso https://orcid.org/0000-0003-4420-5609
Matthias Wessling https://orcid.org/0000-0002-7874-5315

REFERENCES

Alagappan, G., & Cowan, R. M. (2004). Effect of temperature and dissolved oxygen on the growth kinetics of *Pseudomonas putida* F1 growing on benzene and toluene. *Chemosphere*, *54*(8), 1255–1265. https://doi.org/10.1016/j.chemosphere.2003.09.013

Anic, I., Apolonia, I., Franco, P., & Wichmann, R. (2018). Production of rhamnolipids by integrated foam adsorption in a bioreactor system. *AMB Express*, *8*(1), 122. https://doi.org/10.1186/s13568-018-0651-y

Bach, C., Yang, J., Larsson, H., Stocks, S. M., Gernaey, K. V., Albaek, M. O., & Krühne, U. (2017). Evaluation of mixing and mass transfer in a stirred pilot scale bioreactor utilizing CFD. *Chemical Engineering Science*, *171*, 19–26. https://doi.org/10.1016/j.ces.2017.05.001

Bagdasarian, M., Lurz, R., Rückert, B., Franklin, F., Bagdasarian, M., Frey, J., & Timmis, K. (1981). Specific-purpose plasmid cloning vectors II. Broad host range, high copy number, RSF 1010-derived vectors, and a host-vector system for gene cloning in *Pseudomonas*. *Gene*, *16*(1-3), 237–247. https://doi.org/10.1016/0378-1119(81)90080-9

Banat, I. M., Makkar, R. S., & Cameotra, S. S. (2000). Potential commercial applications of microbial surfactants. *Applied Microbiology and Biotechnology*, *53*(5), 495–508. https://doi.org/10.1007/s002530051648

Bator, I., Wittgens, A., Rosenau, F., Tiso, T., & Blank, L. M. (2020). Comparison of three xylose pathways in *Pseudomonas putida* KT2440 for the synthesis of valuable products. *Frontiers in Bioengineering and Biotechnology*, *7*, 480. https://doi.org/10.3389/fbioe.2019.00480

Behrens, B., Baune, M., Jungkeit, J., Tiso, T., Blank, L. M., & Hayen, H. (2016). High performance liquid chromatography- charged aerosol detection applying an inverse gradient for quantification of rhamnolipid biosurfactants. *Journal of Chromatography A*, *1455*, 125–132. https://doi.org/10.1016/j.chroma.2016.05.079

Blesken, C. C., Strümpfler, T., Tiso, T., & Blank, L. M. (2020). Uncoupling foam fractionation and foam adsorption for enhanced biosurfactant synthesis and recovery. *Microorganisms*, *8*(12), 2029. https://doi.org/10.3390/microorganisms8122029

Carstensen, F., Klement, T., Büchs, J., Melin, T., & Wessling, M. (2013). Continuous production and recovery of itaconic acid in a membrane bioreactor. *Bioresource Technology*, *137*, 179–187. https://doi.org/10.1016/j.biortech.2013.03.044

Cazzolla Gatti, R., Liang, J., Velichevskaya, A., & Zhou, M. (2019). Sustainable palm oil may not be so sustainable. *Science of The Total Environment*, *652*, 48–51. https://doi.org/10.1016/j.scitotenv.2018.10.222

Charcosset, C. (2012). *Membrane processes in biotechnology and pharmaceutics*. Elsevier. https://doi.org/10.1016/C2011-0-04261-8

Chong, H., & Li, Q. (2017). Microbial production of rhamnolipids: Opportunities, challenges and strategies. *Microbial Cell Factories*, *16*(1), 137. https://doi.org/10.1186/s12934-017-0753-2

Cote, P., Bersillon, J.-L., & Huyard, A. (1989). Bubble-free aeration using membranes: Mass transfer analysis. *Journal of Membrane Science*, *47*(1-2), 91–106. https://doi.org/10.1016/S0376-7388(00)80862-5

Cote, P., Bersillon, J.-L., Huyard, A., & Faup, G. (1988). Bubble-free aeration using membranes: Process analysis. *Journal (Water Pollution Control Federation)*, 1986–1992.

Coutte, F., Lecouturier, D., Yahia, S. A., Leclère, V., Béchet, M., Jacques, P., & Dhulster, P. (2010). Production of surfactin and fengycin by *Bacillus subtilis* in a bubbleless membrane bioreactor. *Applied Microbiology and Biotechnology*, *87*(2), 499–507. https://doi.org/10.1007/s00253-010-2504-8

Cutayar, J.-M., Poillon, D., & Cutayar, S. (1990). *US Patent No. 4,978,545*. Washington, DC: US Patent and Trademark Office.

Davey, M. E., Caiazza, N. C., & O'Toole, G. A. (2003). Rhamnolipid surfactant production affects biofilm architecture in *Pseudomonas aeruginosa* PAO1. *Journal of Bacteriology*, *185*(3), 1027–1036. https://doi.org/10.1128/jb.185.3.1027-1036.2003

De Almeida, D. G., Soares Da Silva, R. D. C. F., Luna, J. M., Rufino, R. D., Santos, V. A., Banat, I. M., & Sarubbo, L. A. (2016). Biosurfactants: Promising molecules for petroleum biotechnology advances. *Frontiers in Microbiology*, *7*, 1718. https://doi.org/10.3389/fmicb.2016.01718

Delvigne, F., & Lecomte, J.-P. (2009). Foam formation and control in bioreactors. *Encyclopedia of Industrial Biotechnology: Bioprocess, Bioseparation, and Cell Technology*, *121*, 1–13. https://doi.org/10.1002/9780470054581.eib326

Demling, P., von Campenhausen, M., Grütering, C., Tiso, T., Jupke, A., & Blank, L. M. (2020). Selection of a recyclable in situ liquid–liquid extraction solvent for foam-free synthesis of rhamnolipids in a two-phase fermentation. *Green Chemistry*, *22*(23), 8495–8510. https://doi.org/10.1039/D0GC02885A

Deng, L., Guo, W., Ngo, H. H., Zhang, H., Wang, J., Li, J., & Wu, Y. (2016). Biofouling and control approaches in membrane bioreactors. *Bioresource Technology*, *221*, 656–665. https://doi.org/10.1016/j.biortech.2016.09.105

Drioli, E., Curcio, E., & Di Profio, G. (2005). State of the art and recent progresses in membrane contactors. *Chemical Engineering Research and Design*, *83*(3), 223–233. https://doi.org/10.1205/cherd.04203

Fiechter, A. (1992). Biosurfactants: Moving towards industrial application. *Trends in Food Science & Technology*, *3*, 286–293. https://doi.org/10.1016/0167-7799(92)90215-H

Gjermansen, M., Nilsson, M., Yang, L., & Tolker-Nielsen, T. (2010). Characterization of starvation-induced dispersion in *Pseudomonas putida* biofilms: Genetic elements and molecular mechanisms. *Molecular Microbiology*, *75*(4), 815–826. https://doi.org/10.1111/j.1462-2920.2005.00775.x

Gruber, T., Chmiel, H., K¨appeli, O., & Sticher, P. (1993). Integrated process for continuous rhamnolipid biosynthesis, *Biosurfactant* (p. 157).

Gruber, T. (1991). *Verfahrenstechnische Aspekte der kontinuierlichen Produktion von Biotensiden am Beispiel der Rhamnolipide*. Stuttgart: Universität Stuttgart

Gunther, N. W., Nunez, A., Fett, W., & Solaiman, D. K. (2005). Production of rhamnolipids by *Pseudomonas chlororaphis*, a nonpathogenic bacterium. *Applied and Environmental Microbiology*, *71*(5), 2288–2293. https://doi.org/10.1128/AEM.71.5.2288-2293.2005

Hartmans, S., De Bont, J., & Harder, W. (1989). Microbial metabolism of short-chain unsaturated hydrocarbons. *FEMS Microbiology Letters*, *63*(3), 235–264. https://doi.org/10.1016/0378-1097(89)90133-X

Henkel, M., Müller, M. M., Kügler, J. H., Lovaglio, R. B., Contiero, J., Syldatk, C., & Hausmann, R. (2012). Rhamnolipids as biosurfactants from renewable resources: Concepts for next-generation rhamnolipid production. *Process Biochemistry*, *47*(8), 1207–1219. https://doi.org/10.1016/j.procbio.2012.04.018

Henzler, H.-J. (2000). Particle stress in bioreactors, *Influence of stress on cell growth and product formation* (pp. 35–82). Springer. https://doi.org/10.1007/3-540-47865-5

Hoeks, F. W., Van Wees-Tangerman, C., Luyben, K. C. A., Gasser, K., Schmid, S., & Mommers, H. M. (1997). Stirring as foam disruption (SAFD) technique in fermentation processes. *The Canadian Journal of Chemical Engineering*, *75*(6), 1018–1029. https://doi.org/10.1002/cjce.5450750604

Irie, Y., O'toole, G. A., & Yuk, M. H. (2005). *Pseudomonas aeruginosa* rhamnolipids disperse *Bordetella bronchiseptica* biofilms. *FEMS Microbiology Letters*, *250*(2), 237–243. https://doi.org/10.1016/j.femsle.2005.07.012

Junker, B. (2007). Foam and its mitigation in fermentation systems. *Biotechnology Progress*, *23*(4), 767–784. https://doi.org/10.1021/bp070032r

Kosaric, N., & Sukan, F. V. (2014). *Biosurfactants: Production and utilization-processes, technologies, and economics*. CRC Press. https://doi.org/10.1201/b17599

Krishnan, S., Weinman, C. J., & Ober, C. K. (2008). Advances in polymers for anti-biofouling surfaces. *Journal of Materials Chemistry*, *18*(29), 3405–3413. https://doi.org/10.1039/B801491D

de Kronemberger, F. A., Santa Anna, L. M. M., Fernandes, A. C. L. B., de Menezes, R. R., Borges, C. P., & Freire, D. M. G. (2007). Oxygen-controlled biosurfactant production in a bench scale bioreactor, *Biotechnology for fuels and chemicals* (pp. 401–413). Springer. https://doi.org/10.1007/s12010-007-8057-3

Müller, M. M., Hörmann, B., Syldatk, C., & Hausmann, R. (2010). *Pseudomonas aeruginosa* PAO1 as a model for rhamnolipid production in bioreactor systems. *Applied Microbiology and Biotechnology*, *87*(1), 167–174. https://doi.org/10.1007/s00253-010-2513-7

Nelson, K. E., Weinel, C., Paulsen, I. T., Dodson, R. J., Hilbert, H., Martins dos Santos, V. A., Fouts, D. E., Gill, S. R., Pop, M., Holmes, M., Brinkac, L., Beanan, M., DeBoy, R. T., Daugherty, S., Kolonay, J., Madupu, R., Nelson, W., White, O., Peterson, J., … Fraser, C. M. (2002). Complete genome sequence and comparative analysis of the metabolically versatile *Pseudomonas putida* KT2440. *Environmental Microbiology*, *4*(12), 799–808. https://doi.org/10.1046/j.1462-2920.2002.00366.x

Nienow, A. W. (1998). Hydrodynamics of stirred bioreactors. *Applied Mechanics Reviews*, *51*(1), 3–32. https://doi.org/10.1115/1.3098990

Soltani Dashtbozorg, S., Miao, S., & Ju, L.-K. (2016). Rhamnolipids as environmentally friendly biopesticide against plant pathogen *Phytophthora sojae*. *Environmental Progress & Sustainable Energy*, *35*(1), 169–173. https://doi.org/10.1002/ep.12187

Syron, E., & Casey, E. (2008). Membrane-aerated biofilms for high rate biotreatment: Performance appraisal, engineering principles, scale-up, and development requirements. *Environmental Science & Technology*, *42*(6), 1833–1844. https://doi.org/10.1021/es0719428

Tiso, T., Germer, A., Küpper, B., Wichmann, R., & Blank, L. M. (2015). Methods for recombinant rhamnolipid production, *Hydrocarbon and*

lipid microbiology protocols (pp. Springer Protocols Handbooks, 65–94). Berlin, Heidelberg: Springer. https://doi.org/10.1007/8623_2015_60

Tiso, T., Ihling, N., Kubicki, S., Biselli, A., Schonhoff, A., Bator, I., Thies, S., Karmainski, T., Kruth, S., Willenbrink, A. L., Loeschcke, A., Zapp, P., Jupke, A., Jaeger, K. E., Büchs, J., & Blank, L. M. (2020). Integration of genetic and process engineering for optimized rhamnolipid production using *Pseudomonas putida*. *Frontiers in Bioengineering and Biotechnology*, *8*, 976. https://doi.org/10.3389/fbioe.2020.00976

Tiso, T., Zauter, R., Tulke, H., Leuchtle, B., Li, W.-J., Behrens, B., & Blank, L. M. (2017). Designer rhamnolipids by reduction of congener diversity: Production and characterization. *Microbial Cell Factories*, *16*(1), 225. https://doi.org/10.1186/s12934-017-0838-y

Trad, Z., Vial, C., Fontaine, J.-P., & Larroche, C. (2015). Modeling of hydrodynamics and mixing in a submerged membrane bioreactor. *Chemical Engineering Journal*, *282*, 77–90. https://doi.org/10.1016/j.cej.2015.04.119

Vardar-Sukan, F. (1992). Foaming and its control in bioprocesses, *Recent advances in biotechnology* (pp. 113–146). Springer. https://doi.org/10.1007/978-94-011-2468-36

Vlaev, S. D., Tsibranska, I., & Dzhonova-Atanasova, D. (2018). Hydrodynamic characterization of dual-impeller submerged membrane bioreactor relevant to single-use bioreactor options. *Chemical Engineering Research and Design*, *132*, 930–941. https://doi.org/10.1016/j.cherd.2018.02.004

Wittgens, A., Tiso, T., Arndt, T. T., Wenk, P., Hemmerich, J., Müller, C., Wichmann, R., Küpper, B., Zwick, M., Wilhelm, S., Hausmann, R., Syldatk, C., Rosenau, F., & Blank, L. M. (2011). Growth independent rhamnolipid production from glucose using the non-pathogenic *Pseudomonas putida* KT2440. *Microbial Cell Factories*, *10*(1), 80. https://doi.org/10.1186/1475-2859-10-80

Wu, Q., Yan, X., Xiao, K., Guan, J., Li, T., Liang, P., & Huang, X. (2018). Optimization of membrane unit location in a full-scale membrane bioreactor using computational fluid dynamics. *Bioresource Technology*, *249*, 402–409. https://doi.org/10.1016/j.biortech.2017.09.209

Xiao, K., Liang, S., Wang, X., Chen, C., & Huang, X. (2019). Current state and challenges of full-scale membrane bioreactor applications: A critical review. *Bioresource Technology*, *271*, 473–481. https://doi.org/10.1016/j.biortech.2018.09.061

SUPPORTING INFORMATION

Additional Supporting Information may be found online in the supporting information tab for this article.

How to cite this article: Bongartz, P., Bator, I., Baitalow, K., Keller, R., Tiso, T., Blank, L. M., & Wessling, M. (2021). A scalable bubble-free membrane aerator for biosurfactant production. *Biotechnology Bioengineering*. 118, 3545–3558. https://doi.org/10.1002/bit.27822